# Module-Scale Analysis of Pressure Retarded Osmosis: Performance Limitations and Implications for Full-Scale Operation

**ARTICLE** *in* ENVIRONMENTAL SCIENCE AND TECHNOLOGY · SEPTEMBER 2014

Impact Factor: 5.33 · DOI: 10.1021/es503790k · Source: PubMed



**3 AUTHORS:**

Anthony P. Straub
Yale University
**11** PUBLICATIONS **164** CITATIONS
SEE PROFILE

Shihong Lin
Vanderbilt University
**29** PUBLICATIONS **524** CITATIONS
SEE PROFILE

Menachem Elimelech
Yale University
**395** PUBLICATIONS **32,645** CITATIONS
SEE PROFILE

Environmental Science & Technology

Article

pubs.acs.org/est

# Module-Scale Analysis of Pressure Retarded Osmosis: Performance Limitations and Implications for Full-Scale Operation

Anthony P. Straub, Shihong Lin, and Menachem Elimelech*

Department of Chemical and Environmental Engineering, Yale University, New Haven, Connecticut 06520-8286, United States

Supporting Information

**ABSTRACT:** We investigate the performance of pressure retarded osmosis (PRO) at the module scale, accounting for the detrimental effects of reverse salt flux, internal concentration polarization, and external concentration polarization. Our analysis offers insights on optimization of three critical operation and design parameters—applied hydraulic pressure, initial feed flow rate fraction, and membrane area—to maximize the specific energy and power density extractable in the system. For co- and counter-current flow modules, we determine that appropriate selection of the membrane area is critical to obtain a high specific energy. Furthermore, we find that the optimal operating conditions in a realistic module can be reasonably approximated using established optima for an ideal system (i.e., an applied hydraulic pressure equal to approximately half the osmotic pressure difference and an initial feed flow rate fraction that provides equal amounts of feed and draw solutions). For a system in counter-current operation with a river water (0.015 M NaCl) and seawater (0.6 M NaCl) solution pairing, the maximum specific energy obtainable using performance properties of commercially available membranes was determined to be 0.147 kWh per $m^3$ of total mixed solution, which is 57% of the Gibbs free energy of mixing. Operating to obtain a high specific energy, however, results in very low power densities (less than 2 $W/m^2$), indicating that the trade-off between power density and specific energy is an inherent challenge to full-scale PRO systems. Finally, we quantify additional losses and energetic costs in the PRO system, which further reduce the net specific energy and indicate serious challenges in extracting net energy in PRO with river water and seawater solution pairings.

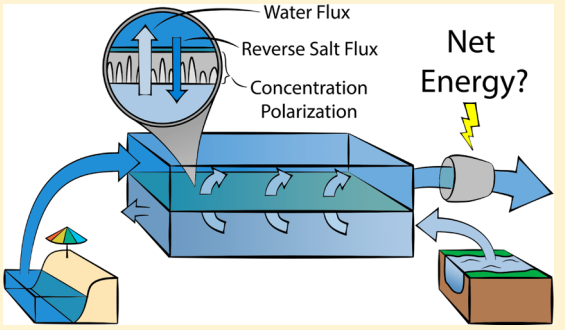


## INTRODUCTION

A global shift in the energy production portfolio toward more renewable sources is critical to reduce greenhouse gas emissions and secure a sustainable future.[1] An emerging source of renewable energy is the salinity gradient energy released upon mixing two solutions of different concentrations.[2,3] The global potential of salinity gradient energy by mixing river water and seawater alone is estimated to be 2 TW.[4] Other promising solution pairings using highly saline solutions, such as reverse osmosis brine or Dead Sea water, as the high concentration streams, have also been proposed.[2,5]

Several feasible technologies have been developed to harness salinity gradient energy, such as pressure retarded osmosis (PRO), reverse electrodialysis, and capacitive mixing.[6−12] Among these, pressure retarded osmosis is the most heavily investigated. In a PRO process, a semipermeable membrane is employed between a low concentration stream (feed solution) and a high concentration stream (draw solution) to allow for controlled mixing. A hydraulic pressure lower than the osmotic pressure difference between the feed and draw solutions is applied on the draw solution side. Water permeates across the membrane from the feed solution to the draw solution, thereby expanding the volume of the pressurized draw solution. The diluted draw solution is partially depressurized through a hydroturbine to generate electricity.[13]

Most existing PRO studies focus on the mass transfer kinetics of a small-scale membrane coupon to understand the membrane properties and power density.[14−18] Although these types of studies are indispensable to gauge the relative performance of different membranes, the energy output and efficiency of the full-scale process must be assessed to determine the overall viability of PRO. In this full-scale process, the effects of constant-pressure operation, draw solution dilution, and feed solution concentration in membrane modules restrict the overall performance of the system. Limited experiments have been conducted to investigate PRO in large-scale modules because of the difficulty in constructing and operating these systems under pressure. Those experiments that have been conducted identified important factors for system design, but encountered challenges in determining an accurate extractable energy.[5,19] Therefore, modeling of the full-scale process using experimentally verified transport equations can be used to determine the viability of real systems and inform their design and operation.

Previous module-scale modeling studies on PRO have evaluated the extractable energy per volume of low-concen-

Received: August 4, 2014
Revised: September 12, 2014
Accepted: September 15, 2014

   dx.doi.org/10.1021/es503790k | Environ. Sci. Technol. XXXX, XXX, XXX−XXX

tration feed solution based on the assumption that fresh water is a limited resource compared to seawater.[20−22] However, using this normalization method does not allow for reasonable optimization of the system, because the highest energy per volume of feed solution will always be obtained when a very small amount of freshwater is being mixed with an infinite source of seawater. Additionally, previous work has suggested that both the feed and the draw solution have economic value because they require pumping and some degree of pretreatment.[23]

We recently presented an analysis that instead evaluates the energy efficiency of the process using specific energy, which is defined as the extracted energy normalized by the total initial volume of feed and draw solutions.[24] Using this performance metric, we analytically determined the optimal operating conditions and maximum specific energy for a module-scale PRO process in co- and counter-current flows with the assumptions of an ideal membrane, perfect hydrodynamics, and sufficient membrane area for the controlled mixing to proceed until completion. Our analysis indicated that the optimal operating conditions in both flow configurations are (i) having equal feed and draw solution flow rates and (ii) applying a hydraulic pressure equal to half of the initial osmotic pressure difference between the feed and draw solutions. Notably, the second condition is also established as necessary to obtain the maximum membrane power density of a small membrane coupon with the same assumptions of an ideal membrane and perfect hydrodynamics.[14]

Although these simple optimal conditions provide useful guidance for process optimization, their accuracy in practical systems is questionable as the idealizing assumptions become invalid.[13] For example, a realistic membrane is not perfectly selective, causing the draw solutes to leak through to the feed solution. In addition, perfect hydrodynamics cannot be achieved in the flow channels or the porous support layer of a realistic membrane, leading to concentration polarization which reduces the driving force across the membrane. Realistic modules will also have a finite membrane area that does not allow for the mixing process to reach completion.

Few module-scale analyses have accounted for the effects of imperfect membranes, concentration polarization, and limited membrane area on the maximal extractable energy and power density. The studies that have included these detrimental effects have not systematically investigated how system operation and design might differ in realistic co- and counter-current modules.[25,26] It is therefore of paramount importance to identify the optimal operating conditions and membrane area in practical PRO systems and to evaluate the detrimental impact of system nonidealities on the membrane power density and the specific energy.

In this study, we analyze the specific energy and membrane power density in PRO with the practical constraints of nonideal membranes and mass transfer limitations. We first examine the power density extractable in a small-scale membrane coupon with the effects reverse salt flux and concentration polarization to identify the optimal operating conditions. This analysis is then scaled up to co- and counter-current flow PRO modules, where draw solution dilution and feed solution concentration substantially decrease the extractable specific energy. The trade-off between increased specific energy and decreased power density with a larger membrane area is evaluated. We also determine the maximum extractable specific energy and corresponding optimal operation parameters for different membrane properties and module designs. The practical implications for PRO are discussed and limitations of the conventional river water and seawater solution pairing are emphasized.

## SYSTEM MODEL OF PRESSURE RETARDED OSMOSIS

We start our analysis by considering the local mass transfer kinetics of water and solutes. These local water and solute fluxes can then be integrated with respect to membrane area along the module to determine full-scale performance. Module operations with both co-current flow and counter-current flow configurations are investigated. Although our primary focus is on the performance in realistic systems, ideal system performance is also included for comparison.

**Ideal Membrane with Perfect Hydrodynamics.** The mass transfer kinetics of water across a semipermeable membrane with a draw solution under applied hydraulic pressure, $\Delta P$, are generally described by

$$J_w = A(\Delta\pi_m - \Delta P) = A(\pi_{D,m} - \pi_{F,m} - \Delta P) \quad (1)$$

where $A$ is the water permeability, $\Delta\pi_m$ is the transmembrane osmotic pressure difference, and $\pi_{D,m}$ and $\pi_{F,m}$ are the osmotic pressures of the draw and feed solutions at the membrane surfaces, respectively.

We first consider an ideal system with a perfectly selective membrane (i.e., allowing only the passage of water molecules but rejecting all solutes) and perfect hydrodynamics in the draw and feed channels so that the concentrations at the membrane surface are equal to the bulk concentrations. With these assumptions, the ideal water flux, $J_{w,i}$, is given by

$$J_{w,i} = A(\Delta\pi - \Delta P) = A(\pi_D - \pi_F - \Delta P) \quad (2)$$

where $\Delta\pi$ is the bulk osmotic pressure difference, and $\pi_D$ and $\pi_F$ are the bulk osmotic pressures of the draw and feed solutions, respectively.

**Realistic Membrane with Reverse Salt Flux and Concentration Polarization.** With a realistic membrane and imperfect hydrodynamics, three phenomena occur to reduce the transmembrane water flux. First, the porous support layer induces internal concentration polarization (ICP), which detrimentally enhances $\pi_{F,m}$ by increasing the solute concentration at the feed-membrane interface and thus reduces the transmembrane driving force. Second, without perfect hydrodynamics in the draw solution flow channel, dilutive external concentration polarization (ECP) develops, which lowers $\pi_{D,m}$ and reduces the driving force. Lastly, because the membrane is no longer perfectly selective, reverse salt flux (RSF) takes place, resulting in uncontrolled mixing and therefore reduced energy extraction in the process.

Solving the full equations for the mass transfer of water and solutes across the membrane with the effects of ICP, ECP, and RSF taken into account, yields the expressions for quantifying realistic water flux, $J_{w,r}$, and salt flux, $J_{s,r}$:[16]

$$J_{w,r} = A\left\{\frac{\pi_D \exp\left(-\frac{J_{w,r}}{k}\right) - \pi_F \exp\left(\frac{J_{w,r}S}{D}\right)}{1 + \frac{B}{J_{w,r}}\left[\exp\left(\frac{J_{w,r}S}{D}\right) - \exp\left(-\frac{J_{w,r}}{k}\right)\right]} - \Delta P\right\} \quad (3)$$


dx.doi.org/10.1021/es503790k | Environ. Sci. Technol. XXXX, XXX, XXX−XXX

$$J_{s,r} = B\left\{\frac{c_D\exp\left(-\frac{J_{w,r}}{k}\right) - c_F\exp\left(\frac{J_{w,r}S}{D}\right)}{1 + \frac{B}{J_{w,r}}\left[\exp\left(\frac{J_{w,r}S}{D}\right) - \exp\left(-\frac{J_{w,r}}{k}\right)\right]}\right\} \quad (4)$$

where $k$ is the mass transfer coefficient of the draw solution−membrane boundary layer, $D$ is the diffusion coefficient of the solute, $S$ is the structural parameter of the membrane support layer, and $B$ is the salt permeability. Because of the inherent permeability-selectivity trade-off of salt rejecting membranes with a polyamide active layer, the $B$ value of the PRO membrane is dependent on the water permeability coefficient $A$ via the correlation equation:[17]

$$B = k_1A^{k_2} \quad (k_1 = 0.0133,\ k_2 = 3) \quad (5)$$

**Mass Transfer in Module Scale Operation.** Practical PRO is operated in full-scale modules that behave significantly different from small membrane coupons. With small membrane coupons, because mass transfer is limited by the available membrane area, the bulk feed and draw concentrations, and thus the osmotic pressure difference, can be approximated as constant. For module-scale operation, however, the osmotic pressures decrease along the flow direction as the draw solution is diluted and the feed solution is concentrated due to simultaneous transport of water and solutes across the membrane.

To better understand the behavior of PRO in a full-scale system, the mass transfer equations for water and solute transport have to be solved for the entire module, which can be done by first solving the flux equations (eqs 3 and 4) for a differential element and then relating the fluxes to changes in the water flow rates and solute concentrations based on mass balance. Here, the performance of two module configurations, co-current and counter-current flow, are studied.

For co-current flow operation, the governing mass transfer equations for water are given in eqs 6A and 6B for the draw and feed solutions, respectively, whereas the solute mass transfer equations are given in eqs 6C and 6D for the draw and feed solutions, respectively:

$$\frac{dQ_D(s)}{ds} = J_{w,r}(c_D(s),\ c_F(s),\ \Delta P) \quad (6A)$$

$$\frac{dQ_F(s)}{ds} = -J_{w,r}(c_D(s),\ c_F(s),\ \Delta P) \quad (6B)$$

$$\frac{d(Q_D(s)c_D(s))}{ds} = -J_{s,r}(c_D(s),\ c_F(s),\ \Delta P) \quad (6C)$$

$$\frac{d(Q_F(s)c_F(s))}{ds} = J_{s,r}(c_D(s),\ c_F(s),\ \Delta P) \quad (6D)$$

Here, $Q_D$ and $Q_F$ are the volumetric flow rates of the draw and feed solutions, respectively, and $c_D$ and $c_F$ are the solute concentrations of the draw and feed solutions, respectively. For generality, we use the relative membrane area, $s$, to represent the position in the module. We define $s$ as the membrane area from the flow entrance to the position being described, normalized by the total membrane area, $A_m$. The boundary conditions for eqs 6A−6D are (i) $Q_D(0) = Q_{D,0}$ and $Q_F(0) = Q_{F,0}$, with $Q_{D,0}$ and $Q_{F,0}$ being the initial draw and feed flow rates, and (ii) $c_D(0) = c_{D,0}$ and $c_F(0) = c_{F,0}$, with $c_{D,0}$ and $c_{F,0}$ being the initial draw and feed solute concentrations.

The mass transfer equations for counter-current flow operation are summarized below:

$$\frac{dQ_D(s)}{ds} = J_{w,r}(c_D(s),\ c_F(s),\ \Delta P) \quad (7A)$$

$$\frac{dQ_F(s)}{ds} = J_{w,r}(c_D(s),\ c_F(s),\ \Delta P) \quad (7B)$$

$$\frac{d(Q_D(s)c_D(s))}{ds} = -J_{s,r}(c_D(s),\ c_F(s),\ \Delta P) \quad (7C)$$

$$\frac{d(Q_F(s)c_F(s))}{ds} = -J_{s,r}(c_D(s),\ c_F(s),\ \Delta P) \quad (7D)$$

These equations are similar to those for co-current flow operation (eqs 6A−6D), except for the signs of $dQ_F(s)/ds$ in eq 7B and $d(Q_F(s)c_F(s))/ds$ in eq 7D, which account for the difference in flow directions. Because the flow directions of the draw and feed solutions are opposite in counter-current flow operation, we arbitrarily define the flow direction of the draw solution as positive and $s$ as the relative distance from the draw solution inlet. The boundary conditions for eqs 7 are $Q_D(0) = Q_{D,0}$, $Q_F(A_m) = Q_{F,0}$, $c_D(0) = c_{D,0}$, and $c_F(A_m) = c_{F,0}$. For eqs 6A−6D and 7A−7D, the positive direction for transmembrane water flux is defined to be from the feed to draw solution, whereas that for the solute flux is defined to be from the draw to the feed solution.

For simplicity and generality of the discussion, we define the initial feed flow rate fraction, $\phi$, as

$$\phi = \frac{Q_{F,0}}{Q_{F,0} + Q_{D,0}} \quad (8)$$

In a module-scale operation, $A_m$ is an important system design parameter, whereas $\phi$ and $\Delta P$ are the two critical operation parameters. A primary objective of current study is to identify the optima for these parameters in a practical PRO operation.

**Quantifying Process Performance.** Two metrics are used to quantify the performance of the PRO process. The first is the membrane power density, PD, defined as the power generated per membrane area. For a small membrane coupon, PD is simply the product of the transmembrane water flux and the applied pressure:

$$PD = J_w\Delta P \quad (9)$$

For a full-scale system, PD varies along the module, and the average power density $\overline{PD}$ is used instead:

$$\overline{PD} = \Delta P\Delta Q/A_m \quad (10)$$

where $\Delta Q$ is the transmembrane water flow rate for the entire module and $A_m$ is the total membrane area.

The second parameter to quantify PRO process performance is the specific energy, SE, defined as the energy extracted per total volume of the feed and draw solutions combined:

$$SE = \frac{\Delta P\Delta Q}{Q_{F,0} + Q_{D,0}} \quad (11)$$

We note that SE can also be interpreted as the energy density of the combined solutions. While PD measures how fast the energy is being converted, SE quantifies the amount of energy extracted from the process.


dx.doi.org/10.1021/es503790k | Environ. Sci. Technol. XXXX, XXX, XXX−XXX

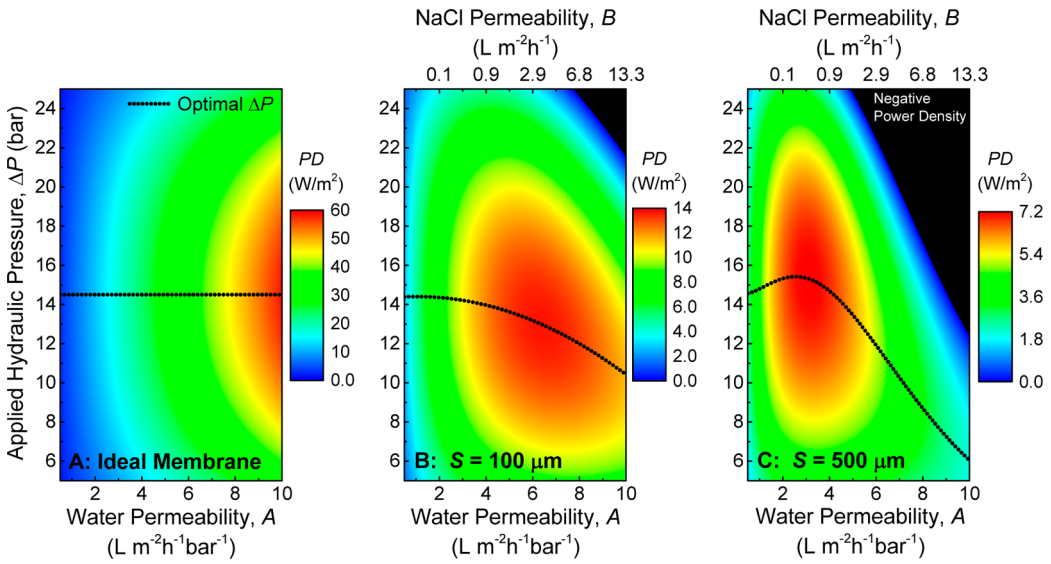


**Figure 1.** Areal coupon-scale power density at different applied hydraulic pressures, $\Delta P$, and water permeabilities, $A$, for (A) ideal membranes with perfect hydrodynamics, (B) realistic membranes with a structural parameter, $S$, of 100 $\mu$m, and (C) realistic membranes with $S$ = 500 $\mu$m. The salt permeability coefficient, $B$, in panels B and C is correlated with the water permeability coefficient, $A$, based on the permeability-selectivity trade-off (eq 5). ECP is not considered in panel A, but considered in panels B and C with a mass transfer coefficient of $k$ = 138.6 L m$^{-2}$ h$^{-1}$. The black dotted curves represent the optimal applied hydraulic pressure leading to maximum power density for a given water permeability. A seawater draw solution (0.6 M NaCl) and river water feed solution (0.015 M NaCl) are used.

**Assumptions in PRO System Modeling.** Our analysis of the PRO process outlined above uses several idealizing assumptions to simplify the modeling and allow for more intuitive interpretation of the results. We assume no pressure loss due to pumping of solutions through the feed and draw channels. We also do not consider factors beyond the membrane module, such as inefficiencies in the pressure exchanger or turbine. The contribution of these factors is discussed further in the Implications. We also assume a constant draw channel mass transfer coefficient, $k$, throughout the module. All calculations use a value of $k$ = 38.5 $\mu$m (138.6 L m$^{-2}$ h$^{-1}$), which has been established previously in literature and is comparable to experimentally determined values.[17,27] However, it is important to note that this is merely a representative draw mass transfer coefficient and may change based on the flow channel design and operation. A linear relationship between molar concentration and osmotic pressure is assumed using the van't Hoff equation. For the relatively low concentrations used in this work (less than 0.6 M NaCl), the osmotic pressures predicted by the van't Hoff equation will not deviate from those determined by OLI stream analyzer by more than 10%.

## POWER DENSITY IN COUPON-SCALE OPERATION

We begin with examining the power density extractable in a small-scale membrane coupon, which is scaled up to the more practical module (full-scale) operation in the next section. Figure 1 shows the power density, PD, for both ideal (Figure 1A) and realistic (Figure 1B,C) membranes as a function of applied hydraulic pressure, $\Delta P$, and membrane properties. As mentioned earlier, the water permeability, $A$, is linked to the salt permeability, $B$, by the permeability-selectivity trade-off (eq 5). The draw solution concentration is 0.6 M NaCl to represent seawater and the feed concentration is 0.015 M NaCl to represent river water or wastewater effluent, which is the concentration pair for all simulations throughout this paper.

For an ideal membrane ($B$ = 0), the optimal applied pressure, $\Delta P_{opt}$, is simply $\Delta\pi/2$ (Figure 1A), and the corresponding maximum power density, $PD_{max}$, is $A\Delta\pi^2/4$ based on eqs 2 and 9. PD increases with increasing water permeability, with the highest PD shown approaching 58.4 W/m$^2$ when $A$ = 10 L m$^{-2}$ h$^{-1}$ bar$^{-1}$. For realistic membranes, however, $\Delta P_{opt}$ is no longer $\Delta\pi/2$, but instead dependent on the membrane properties. With a structural parameter $S$ = 100 $\mu$m, which may be attained with advanced, state-of-the-art PRO membranes,[28,29] $\Delta P_{opt}$ decreases with increasing $A$ (and correspondingly increasing $B$) values. PD reaches a maximum of 13.7 W/m$^2$ with an $A$ value of 6.4 L m$^{-2}$ h$^{-1}$ bar$^{-1}$ and a corresponding $\Delta P_{opt}$ of 13 bar. With a higher structural parameter $S$ = 500 $\mu$m that is more typical for current PRO membranes,[27,30,31] PD reaches a maximum at an $A$ value of 3.1 L m$^{-2}$ h$^{-1}$ bar$^{-1}$and $\Delta P_{opt}$ of 15.4 bar, leading to a $PD_{max}$ of 7.2 W/m$^2$.

The reduction of PD with increasing $S$ value is attributable to the exacerbated ICP, which significantly reduces the driving force. Comparing Figure 1B and Figure 1C also suggests that enhancing water permeability of a membrane beyond a certain limit does not increase $PD_{max}$, unless $S$ can be reduced at the same time. In fact, due to the effects of both RSF and ICP, the water flux can become negative (i.e., from the draw solution to the feed solution) with a nonideal membrane of a high $A$ value, even if $\Delta P$ is still lower than $\Delta\pi$. Although $\Delta P_{opt}$ is not exactly $\Delta\pi/2$, but rather dependent on the membrane properties, the data used in Figure 1B,C demonstrates that using $\Delta P = \Delta\pi/2$ (in this case ≈14.5 bar) for typical water permeabilities ($A$ < 5 L m$^{-2}$ h$^{-1}$ bar$^{-1}$) would allow for at least 99% of $PD_{max}$ to be obtained. Therefore, it is convenient to apply a pressure of $\Delta\pi/2$ in practice to approach $PD_{max}$ at the membrane coupon scale.

## MODULE-SCALE PERFORMANCE WITH REALISTIC MEMBRANES AND CONCENTRATION POLARIZATION

A coupon-scale analysis provides information about the kinetics of energy production and is relevant only to small, lab-scale tests. To understand both the kinetics and energy efficiency in a


dx.doi.org/10.1021/es503790k | Environ. Sci. Technol. XXXX, XXX, XXX−XXX

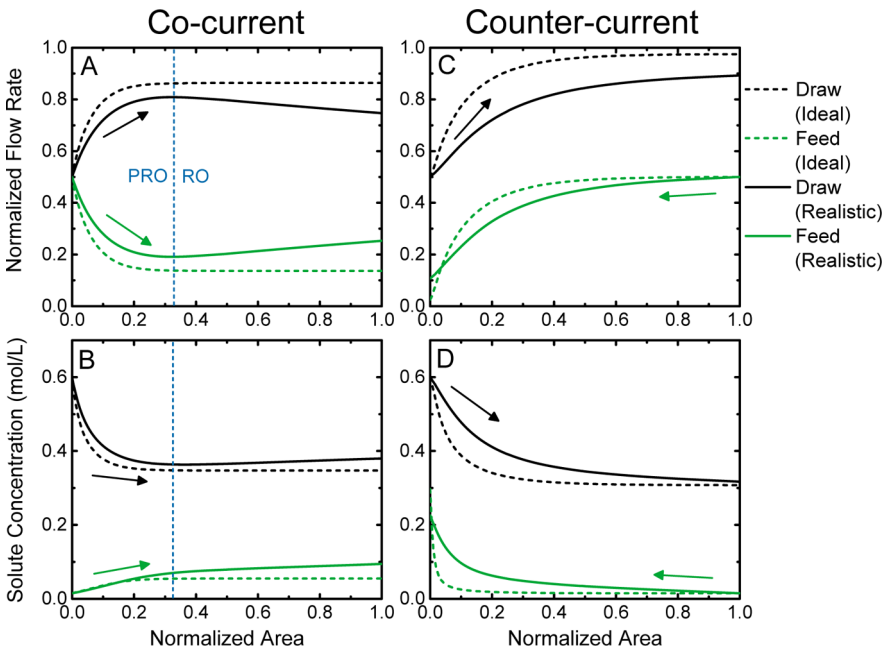


**Figure 2.** Distributions of normalized flow rates (A and C) and solute concentrations (B and D) in a PRO module in both co-current flow mode (A and B) and counter-current flow mode (C and D). The dashed curves represent an ideal scenario without reverse salt flux and concentration polarization. The solid curves represent a realistic scenario with reverse salt flux, internal concentration polarization, and external concentration polarization all considered. The feed solution is river water (0.015 M) and the draw solution is seawater (0.6 M). Arrows show the direction of flow for each solution. The normalized membrane area $A_m/Q_{F,0}$ = 0.2 m$^2$ h L$^{-1}$ and the applied pressure $\Delta P$ = 14.5 bar ($\Delta\pi/2$). The membrane properties are $A$ = 3 L m$^{-2}$ h$^{-1}$ bar$^{-1}$, $B$ = 0.36 L m$^{-2}$ h$^{-1}$ (determined with eq 5), and $S$ = 100 $\mu$m. ECP is also considered with a mass transfer coefficient of $k$ = 138.6 L m$^{-2}$ h$^{-1}$. The blue dashed lines indicate a critical position that divides the co-current module into two regimes: the trans-membrane water flux is positive (toward the draw solution) in the regime left of the critical position (i.e., PRO operation) and is negative in the regime right of the critical position (i.e., RO operation). Excessive membrane area was deliberately used in the simulations to demonstrate the existence of negative water flux in co-current flow.

practical PRO system, a module-scale analysis must be conducted. This analysis can be carried out by numerically solving the mass balance equations for co-current and counter-current flow (eqs 6A−6D and 7A−7D, respectively) and the governing equations for water and salt flux (eqs 3 and 4) along the length of the module. In the following subsections, results from this modeling are used to understand the behavior in a module and to explore the effect of membrane area, an important system design parameter, on the specific energy, SE, and average power density, $\overline{PD}$.

**PRO Module Behavior.** The flow rate and concentration distributions for module-scale operation are shown in Figure 2 for an ideal membrane (dashed lines) and a realistic membrane with concentration polarization (solid lines) for co-current (Figure 2A,B) and counter-current (Figure 2C,D) flow configurations. The flow rate distributions (Figure 2A,C) are presented as the normalized flow rate (i.e., flow rate at a given position divided by the total initial flow rate). These normalized flow rate profiles will remain identical regardless of the actual magnitude of the flow rate, so long as the ratio of the membrane area to initial feed flow rate ($A_m/Q_{F,0}$) remains constant. The increase in flow rate of the draw solution is directly proportional to the specific energy obtainable in the process (eq 11), because any change in the draw solution flow rate is due to permeation through the membrane ($\Delta Q$). The solute concentration distribution (Figure 2B,D) is shown for initial concentrations of a model seawater draw solution (0.6 M NaCl) and a river water feed solution (0.015 M NaCl). The difference in concentration between the feed and draw solution at a given position is representative of the driving force available from the bulk solutions.

Observing the distributions in co-current flow operation, the detrimental effects of ICP, ECP, and RSF are readily apparent. The permeation of water through the membrane near the entrance of the module, represented by the change in flow rate profiles (Figure 2A), is noticeably lower in the realistic scenario than the idealized scenario due to a reduction in driving force (eqs 3 and 4). After the initial permeation of water from the feed to the draw solution, the realistic co-current module reaches a critical position that divides the module into two distinct regimes: the transmembrane water flux is positive in the regime prior to the critical position (i.e., PRO regime) and is negative in the regime following the critical position (i.e., reverse osmosis or RO regime). The draw solution flow rate reaches its maximum at the critical position and mass transfer beyond this point serves to reduce the draw solution flow rate (and therefore the specific energy obtained in the module). At the critical position, less water has permeated through the module in the realistic scenario than in the ideal scenario due to uncontrolled mixing across the membrane (i.e., reverse salt flux). An excessive membrane area was deliberately used in the simulation to demonstrate the existence of negative water flux in co-current flow. In practical operation, as will be discussed in the following section, modules would be designed to avoid the emergence of the RO regime.

In counter-current flow operation, the effects of realistic factors on membrane performance are less straightforward. From the normalized flow rate distributions (Figure 2C), it is clear the realistic scenario has reduced permeation of water across the membrane module compared to the ideal case due to RSF and concentration polarization. However, unlike co-current flow operation, all of the membrane area is utilized for power generation (i.e., the flux is always positive across the membrane).


dx.doi.org/10.1021/es503790k | Environ. Sci. Technol. XXXX, XXX, XXX−XXX

Even if the membrane area is increased dramatically, none of the membrane area in the counter-current module will enter the RO regime (data not shown). This can be explained by the fact that the effects of draw solution dilution and feed solution concentration occur in opposite directions. Therefore, each solution will have to undergo a larger concentration change in order for flux reversal to occur.

**Effect of Membrane Area on Specific Energy and Power Density.** The preceding subsection identified that reverse salt flux can lead to regions in the module that contribute negatively to the specific energy. Modules must therefore be designed to reduce this effect to maximize the efficiency of energy extraction. The total membrane area, $A_m$, is a critical design parameter, as it largely determines the extent of mass transfer in a given PRO system. Figure 3 shows the specific energy as a function of $A_m$ for co-current and counter-current modules using a river water (0.015 M NaCl) and seawater (0.6 M NaCl) solution pairing. Results are shown for an ideal membrane (dotted lines) and a realistic membrane with RSF, ECP, and ICP (solid lines). For generality, values for $A_m$ are shown normalized by the feed flow rate, $Q_{F,0}$, because both these parameters will determine the extent of mass transfer in the process.

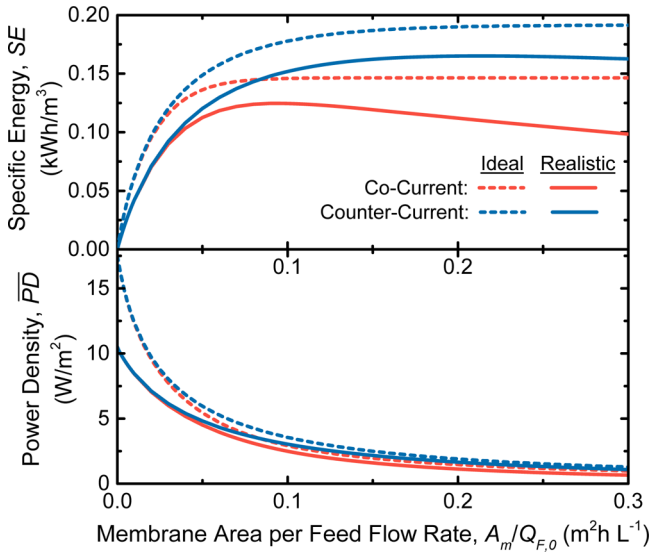


**Figure 3.** Specific energy (top) and average power density (bottom) as functions of the membrane area normalized by feed flow rate ($A_m/Q_{F,0}$) for co-current flow mode (red) and counter-current flow mode (blue). Dashed curves represent an ideal scenario without reverse salt flux and concentration polarization. Solid curves represent a more realistic scenario with reverse salt flux, ICP, and ECP all considered. The feed solution is river water (0.015 M NaCl) and the draw solution is seawater (0.6 M NaCl). The applied pressure $\Delta P$ = 14.5 bar ($\Delta\pi/2$), the initial feed flow rate fraction $\phi$ = 0.5, and the draw mass transfer coefficient $k$ = 138.6 L m$^{-2}$ h$^{-1}$. For the realistic case, the membrane properties are $A$ = 3 L m$^{-2}$ h$^{-1}$ bar$^{-1}$, $B$ = 0.36 L m$^{-2}$ h$^{-1}$ (determined with eq 5), and $S$ = 100 $\mu$m. The coupon-scale power density for each membrane occurs at the power density axis intercept where membrane area approaches zero.

For co-current operation in the ideal case, as $A_m$ increases, SE asymptotically approaches the thermodynamic limit of obtainable specific energy, which has been analytically determined in our recent work to be 0.156 kWh/m$^3$ for a river water and seawater solution pairing.[24] In the realistic case, SE for any module size is always lower than the ideal case due to the effects of RSF, ICP, and ECP. The realistic scenario also has an optimal membrane area, $A_{m,opt}$, where SE is maximized. For the membrane used in Figure 3, $A_{m,opt}$ is reached at $A_m/Q_{F,0}$ = 0.09 m$^2$ h L$^{-1}$ and the corresponding SE is 0.125 kWh/m$^3$. This optimum occurs when the solutions exiting the module have an osmotic pressure difference equal to the hydraulic pressure difference and the driving force has completely vanished ($\Delta\pi = \Delta P$ at end of the module). If $A_m$ is less than $A_{m,opt}$, the process terminates before the driving force has been exhausted (i.e., $\Delta\pi > \Delta P$ for all positions in the module). If $A_m$ is increased beyond $A_{m,opt}$, the concentration build-up due to RSF will reverse the net driving force and water flux will permeate from the draw to the feed solution ($\Delta\pi < \Delta P$), as in the reverse osmosis regime established in the previous section. This implies that any additional membrane area beyond $A_{m,opt}$ serves to decrease the obtainable energy in the process.

In counter-current operation with RSF and concentration polarization, the system also reaches an optimal membrane area where SE is maximized. The optimal membrane area in counter-current flow occurs when $A_m/Q_{F,0}$ = 0.21 m$^2$ h L$^{-1}$, a value larger than that of co-current flow. Counter-current flow also extracts a higher SE (0.165 kWh/m$^3$). Although SE decreases when $A_m$ is larger than $A_{m,opt}$, this is not necessarily due to the existence of a portion of the module with negative transmembrane water flux, highlighting an important distinction between counter-current and co-current operations in a realistic membrane module. Because the solutions flow in opposite directions in counter-current operation, the existence of RSF will diminish the bulk driving force available for permeation across the entire module. This effect increases as the module size increases, eventually to a point where the benefits of additional membrane area for water permeation are outweighed by the detrimental effects of uncontrolled mixing.

The analysis above identifies an optimal membrane area to extract the highest SE from a given module. However, in addition to efficiently extracting the energy available from mixing the feed and draw solutions, it is essential for a practical PRO system to effectively utilize the membrane area (i.e., achieve a high power density). Unlike SE, the average power density of a module, $\overline{PD}$, decreases dramatically as membrane area increases (Figure 3, bottom), indicating an inherent trade-off between $\overline{PD}$ and SE in PRO. Increasing the membrane area dilutes the draw solution and concentrates the feed solution, reducing the average driving force for permeation in the module. However, such reduction of the driving force is an inevitable consequence of the energy extraction needed to obtain a high SE. Indeed, in the highest efficiency scenario (reversible mixing), the draw and feed solution would reach an equal concentration and the kinetics of operation would be infinitely slow ($\overline{PD}$ approaches zero).[22]

Optimizing the membrane area to most appropriately balance $\overline{PD}$ and SE requires a detailed analysis of their relative economic importance, which is complex and beyond the scope of this study. However, it is clear that for any given membrane area, $\overline{PD}$ and SE are both higher in counter-current operation than in co-current operation, and $\overline{PD}$ will be severely reduced at high SE. For the realistic membrane in Figure 3, the power density at the smallest membrane area (i.e., coupon scale when $A_m/Q_{F,0}$ approaches zero) is 10.5 W/m$^2$. At the optimal membrane area to obtain the maximum SE, $\overline{PD}$ is reduced to 1.6 W/m$^2$, which is only 15% of the coupon-scale power density that could be obtained in lab-scale experiments. For system operation with $\overline{PD}$ equal to approximately half of the coupon-scale PD (5.2 W/m$^2$), the SE


dx.doi.org/10.1021/es503790k | Environ. Sci. Technol. XXXX, XXX, XXX−XXX

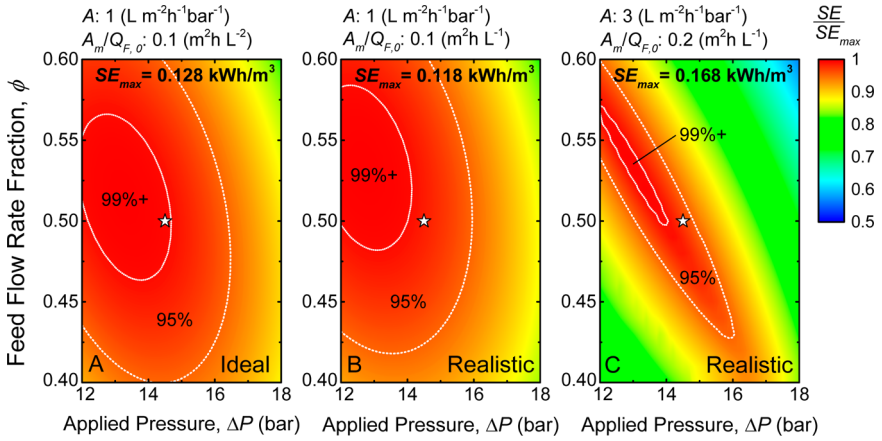


**Figure 4.** Normalized specific energy in counter-current flow mode as a function of feed flow rate fraction and applied hydraulic pressure for an ideal membrane with limited membrane area (A) and realistic membranes (B and C). In these plots, the specific energy, SE, is normalized by the corresponding maximum specific energy of a given module, $SE_{max}$, which is indicated for each case. For realistic membranes, reverse salt flux, internal concentration polarization, and external concentration polarization are all considered with a structural parameter, $S$, of 100 $\mu$m and a mass transfer coefficient of $k = 138.6$ L m$^{-2}$ h$^{-1}$. The feed solution is river water (0.015 M NaCl) and the draw solution is seawater (0.6 M NaCl). Other parameters for the calculations (membrane permeability, $A$, and membrane area normalized by feed flow rate, $A_m/Q_{F,0}$), are given on each subfigure. The inner and the outer circles (white dotted) represent the conditions that yield a specific energy of 99% and 95% of $SE_{max}$. The white star indicates the global optimal condition with an ideal membrane and sufficient membrane area for the process to proceed to completion (i.e., $\phi = 0.5$, $\Delta P = \Delta\pi/2$).

obtainable is reduced to 0.111 kWh/m$^3$ (67% of that obtainable at the optimal membrane area).

## OPTIMAL OPERATING CONDITIONS TO MAXIMIZE ENERGY EXTRACTION

Our analysis of specific energy for different membrane areas uses the optimal operating conditions of an ideal process (i.e., $\phi = 0.5$ and $\Delta P = \pi/2$).[24] However, as was demonstrated with the analysis of coupon-scale power density in Figure 1, reverse salt flux and concentration polarization can lead to a change in the optimal operating parameters of the system. In coupon-scale operation, the only operation parameter is the applied hydraulic pressure, $\Delta P$. However, when a membrane module with given membrane properties and normalized membrane area is operated, both $\Delta P$ and the initial feed flow rate fraction, $\phi$, can be modified to maximize the specific energy. This section investigates the optimal operating conditions and maximum specific energy for different membrane modules.

In Figure 4, we evaluate the optimal operating conditions for three counter-current flow membrane modules. The first module is representative of an ideal membrane with perfect selectivity and ideal hydrodynamics, but a limited membrane area (Figure 4A). The next two modules shown obey the permeability-selectivity trade-off and have concentration polarization at the membrane surface ($S = 100$ $\mu$m and $k = 138.6$ L m$^{-2}$ h$^{-1}$ for both cases). Figure 4B is representative of a case where the process is limited by membrane area, whereas Figure 4C is representative of a case near the optimal membrane area, $A_{m,opt}$, for counter-current operation that was established in Figure 3. For each scenario, SE is evaluated as a function of both $\Delta P$ and $\phi$. In all three cases described in Figure 4, it is clear that the optimal operating conditions that lead to the highest SE deviate from those of an ideal scenario with infinite membrane area ($\Delta P = \pi/2$ and $\phi = 0.5$). For the counter-current modules shown in Figure 4, the optimal applied hydraulic pressure, $\Delta P_{opt}$, is generally around 12.5 bar compared to 14.5 bar for an ideal membrane with infinite membrane area. The optimal feed flow rate fraction, $\phi_{opt}$, ranges from 0.51 to 0.53. With the same modules operating in co-current flow mode (Figure S1, Supporting Information), the optimal operating conditions are similar, with $\Delta P_{opt}$ slightly lower than the ideal condition of $\Delta P = \pi/2$ and $\phi_{opt}$ near 0.5. Co-current operation, however, always results in a lower SE.

The numerical simulations required to determine the absolute optimal operating conditions are time-consuming and computationally intensive. The analysis above, which encompasses most of relevant membrane parameters and module sizes for practical PRO operation, shows that using $\phi = 0.5$ and $\Delta P = \pi/2$ (i.e., the optimal operating conditions in the ideal case where the process proceeds until completion) would allow for at least 95% of the maximum specific energy to be obtained. Additionally, the optimal operating conditions, unlike membrane area, are identical to maximize both specific energy and average power density for a given module (eqs 10 and 11). This means that for most practical cases with the goal of maximizing the average power density and specific energy in a module, the operating conditions can be approximated as $\phi = 0.5$ and $\Delta P = \pi/2$ and do not require extensive simulations.

## IMPLICATIONS

In the preceding analysis, we determined the optimal operation and design parameters to achieve the maximum specific energy in a PRO module with imperfect membranes and concentration polarization. We established that in order to maximize the specific energy in a PRO system with reverse salt flux, the module must be designed so that there is enough area for a substantial amount of controlled mixing to occur, but not so much area that reverse salt flux buildup negatively affects the extractable specific energy. The optimal membrane area is dependent on many different factors and must be determined numerically for a given system design. Optimization of the operation conditions of a PRO system (i.e., the initial flow rate fraction, $\phi$, and applied hydraulic pressure, $\Delta P$), was shown to lead to a relatively minor improvement in the specific energy compared to using $\phi = 0.5$ and $\Delta P = \pi/2$, the optimal operating conditions for an ideal module with infinite membrane area. For most practical purposes, these ideal conditions can be used without conducting extensive numerical simulations.


dx.doi.org/10.1021/es503790k | Environ. Sci. Technol. XXXX, XXX, XXX−XXX

The maximum specific energy and average power density for different membranes are shown in Figure 5. Three different types

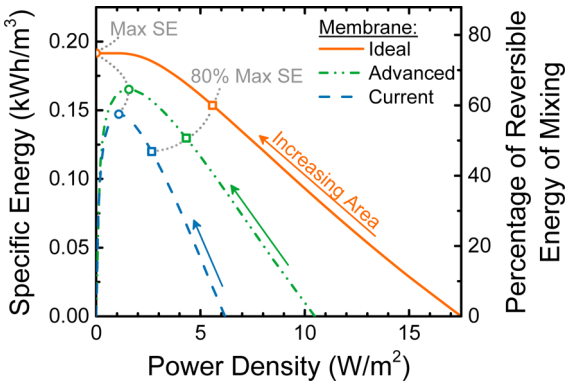


**Figure 5.** Specific energy vs power density for three different types of counter-current modules: an ideal module with no reverse salt flux or concentration polarization (solid red line), a module using advanced membranes (dashed and dotted green line), and a module using currently available commercial membranes (dashed blue line). The ideal membrane has a water permeability coefficient, $A$, of 3 L m$^{-2}$ h$^{-1}$ bar$^{-1}$ and $B$ = 0. For the advanced membrane, $A$ = 3 L m$^{-2}$ h$^{-1}$ bar$^{-1}$, $B$ = 0.36 L m$^{-2}$ h$^{-1}$ (determined from the permeability-selectivity trade-off, eq 5), and $S$ = 100 $\mu$m. The commercial membrane properties are representative of a thin-film composite membrane from Hydration Technology Innovations ($A$ = 2.49 L m$^{-2}$ h$^{-1}$ bar$^{-1}$, $B$ = 0.39 L m$^{-2}$ h$^{-1}$, and $S$ = 564 $\mu$m). In both cases with concentration polarization, a mass transfer coefficient of $k$ = 138.6 L m$^{-2}$ h$^{-1}$ is used. The feed solution is river water (0.015 M NaCl) and the draw solution is seawater (0.6 M NaCl). Curves are obtained by increasing the membrane area with fixed operating conditions of $\phi$ = 0.5 and $\Delta P$ = 14.5 bar. For each membrane, the maximum specific energy (hollow circle) and 80% of the maximum specific energy (hollow square) are indicated. The coupon-scale power density for each membrane occurs at the horizontal axis (power density) intercept.

of membrane modules operating in counter-current flow are shown: an ideal membrane with no reverse salt flux or concentration polarization, an advanced state-of-the-art membrane with a low structural parameter and relatively high water permeability ($A$ = 3 L m$^{-2}$ h$^{-1}$ bar$^{-1}$, $B$ = 0.36 L m$^{-2}$ h$^{-1}$, $S$ = 100 $\mu$m), and membrane representative of current commercially available thin-film composites from Hydration Technology Innovations ($A$ = 2.49 L m$^{-2}$ h$^{-1}$ bar$^{-1}$, $B$ = 0.39 L m$^{-2}$ h$^{-1}$, $S$ = 564 $\mu$m).[27] For a PRO system modeled using parameters from current commercially available membranes, the maximum specific energy available at the optimal membrane area is 0.147 kWh/m$^3$ (57% of the Gibbs free energy of mixing for river water and seawater[24]). With advanced, state-of-the-art membranes with some of the more favorable properties we can expect from current membrane technology, the extractable specific energy can be increased to 0.165 kWh/m$^3$ (64% of the Gibbs free energy of mixing). This indicates that significantly improved membrane properties allow for relatively small gains in specific energy extraction. Even if a membrane can be developed with near perfect selectivity and minimal concentration polarization, the specific energy can only approach 0.192 kWh/m$^3$ (75% of the Gibbs free energy of mixing), which can be obtained with an ideal membrane and sufficient membrane area for the process to reach completion.[24]

To obtain the maximum specific energy with any type of membrane, a relatively large membrane area must be used, severely reducing the power density obtainable. As shown in Figure 5, at the maximum specific energy for the current commercial membranes and the advanced membranes, the power densities are 1.1 and 1.6 W/m$^2$, respectively. For both membrane types, this is about 15% of the power density available at the coupon scale (6.2 and 10.5 W/m$^2$ for commercial and advanced membranes, respectively) and well below the threshold of 5 W/m$^2$ that Statkraft, the Norwegian company that pioneered PRO development, claimed would allow the process to be economically viable.[32] Even if a system is operated at a lower specific energy, for example 80% of the maximum specific energy of a given module, the power density of these membranes will remain below 5 W/m$^2$. This highlights an important challenge for PRO mixing seawater and river water solutions: in order to operate at reasonably high efficiencies, the power density will be low, even with relatively optimistic membrane properties.

Although the analysis in this work accounts for imperfectly selective membranes and mass transfer limitations relevant to PRO, it does not take into account losses that would result from inefficiencies in the pressure exchanger and hydro-turbine. Additionally, energetic costs will be associated with operation of the system. These energetic costs include the pumping required to drive the feed and draw solutions through the narrow membrane channels. On the basis of the pressure drop in experimental PRO modules, we can estimate the energy of pumping to range from 0.01 to 0.12 kWh/m$^3$.[5,19] Colloidal, organic, and biological fouling can also significantly reduce the membrane water flux and decrease the efficiency of the process.[33−35] Even though membrane cleaning methods are in development, it is likely foulants will need to be removed from the source waters before entering the membrane modules.[35] Although the associated energetic cost of pretreatment has not been established for PRO, seawater RO pretreatment (0.12−0.42 kWh/m$^3$)[36,37] and conventional fresh water treatment (0.03−0.73 kWh/m$^3$, with the upper limit accounting for the production energy of chemicals expended)[38−40] can be used to understand the magnitude. It is beyond the scope of this study to thoroughly analyze each of these additional energetic costs, but it is reasonable to assume that they will substantially reduce the net specific energy extractable and may even render the process energy negative. Even with significant improvements to membrane properties and system design, a situation where a sizable energy is extractable using the limited driving force available from mixing river water and seawater may be unlikely.

Alternative solution pairings, such as a desalination plant brine paired with wastewater effluent, offer greater concentration differences and thus higher driving forces for power generation.[13,41,42] In our previous theoretical work examining ideal constant-pressure PRO, we identified that by using higher concentration gradients, the specific energy extractable can be more than twice as high as that of the river water and seawater solution pairing.[24] Although certain losses in PRO, such as those associated with reverse salt flux, will increase with these higher concentration gradients, the energetic costs of pretreatment will likely remain similar and may even decrease with alternative solution pairings. We can therefore postulate that, using these alternative solutions with higher concentration differences, a significant net specific energy may still be obtained in PRO.

## ■ ASSOCIATED CONTENT

### Supporting Information

Details on the optimal operating conditions for co-current flow in different modules (Figure S1). This material is available free of charge via the Internet at http://pubs.acs.org.

## AUTHOR INFORMATION


### Corresponding Author

*M. Elimelech. E-mail: menachem.elimelech@yale.edu. Tel.: +1 (203) 432-2789.


### Notes

The authors declare no competing financial interest.

## ACKNOWLEDGMENTS

We acknowledge the support received from the National Science Foundation under Award Number CBET 1232619 and the partial support from the Advanced Research Projects Agency-Energy (ARPA-E), U.S. Department of Energy, via Grant DE-AR0000306. We also acknowledge the National Science Foundation Graduate Research Fellowship awarded to A.P.S.

## NOMENCLATURE

| | |
|---|---|
| $A$ | water permeability coefficient of the membrane active layer |
| $A_m$ | membrane area |
| $A_{m,opt}$ | optimal membrane area to maximize specific energy |
| $B$ | solute permeability coefficient of the membrane active layer |
| $c$ | solute concentration |
| $D$ | solute diffusion coefficient |
| $J$ | flux |
| $k$ | mass transfer coefficient at the draw solution and active layer interface |
| $\Delta P$ | hydraulic pressure difference across the membrane |
| $\Delta P_{opt}$ | optimal applied hydraulic pressure difference across the membrane |
| PD | power density of a membrane coupon |
| $\overline{PD}$ | average power density of a module |
| $PD_{max}$ | maximum power density of a membrane coupon |
| $Q$ | flow rate |
| $\Delta Q$ | permeate flow rate across the membrane |
| $S$ | structural parameter of the membrane support layer |
| SE | specific energy or extractable energy divided by the total volume of feed and draw solutions |

### Greek Symbols

| | |
|---|---|
| $\pi$ | osmotic pressure |
| $\Delta\pi$ | osmotic pressure difference across the membrane |
| $\phi$ | feed flow rate fraction or feed flow rate divided by the total initial flow rate of feed and draw solutions |
| $\phi_{opt}$ | optimal feed flow rate fraction to maximize specific energy |

### Subscripts

| | |
|---|---|
| 0 | initial condition |
| D | draw solution |
| F | feed solution |
| i | ideal |
| m | membrane active layer interface |
| r | realistic or with the effects of concentration polarization and reverse salt flux |
| s | solute species |
| w | water species |

## REFERENCES


(1) Hoffert, M. I.; Caldeira, K.; Benford, G.; Criswell, D. R.; Green, C.; Herzog, H.; Jain, A. K.; Kheshgi, H. S.; Lackner, K. S.; Lewis, J. S.; et al. Advanced technology paths to global climate stability: Energy for a greenhouse planet. *Science* **2002**, *298*, 981−987.

(2) Logan, B. E.; Elimelech, M. Membrane-based processes for sustainable power generation using water. *Nature* **2012**, *488*, 313−319.

(3) Pattle, R. E. Production of electric power by mixing fresh and salt water in the hydroelectric pile. *Nature* **1954**, *174*, 660.

(4) Mantia, F. La; Pasta, M.; Deshazer, H. Batteries for efficient energy extraction from a water salinity difference. *Nano Lett.* **2011**, *11*, 1810−1813.

(5) Achilli, A.; Prante, J. L.; Hancock, N. T.; Maxwell, E. B.; Childress, A. E. Experimental results from RO-PRO: A next generation system for low-energy desalination. *Environ. Sci. Technol.* **2014**, *48*, 6437−6443.

(6) Helfer, F.; Lemckert, C.; Anissimov, Y. G. Osmotic power with pressure retarded osmosis: Theory, performance and trends—A review. *J. Membr. Sci.* **2014**, *453*, 337−358.

(7) Ramon, G. Z.; Feinberg, B. J.; Hoek, E. M. V. Membrane-based production of salinity-gradient power. *Energy Environ. Sci.* **2011**, *4*, 4423−4434.

(8) Loeb, S. Osmotic power plants. *Science* **1975**, *189*, 654−655.

(9) Post, J. W.; Veerman, J.; Hamelers, H. V. M; Euverink, G. J. W.; Metz, S. J.; Nymeijer, K.; Buisman, C. J. N. Salinity-gradient power: Evaluation of pressure-retarded osmosis and reverse electrodialysis. *J. Membr. Sci.* **2007**, *288*, 218−230.

(10) Yip, N. Y.; Vermaas, D. a.; Nijmeijer, K.; Elimelech, M. Thermodynamic, energy efficiency, and power density analysis of reverse electrodialysis power generation with natural salinity gradients. *Environ. Sci. Technol.* **2014**, *48*, 4925−4936.

(11) Hatzell, M. C.; Cusick, R. D.; Logan, B. E. Capacitive mixing power production from salinity gradient energy enhanced through exoelectrogen-generated ionic currents. *Energy Environ. Sci.* **2014**, *7*, 1159−1165.

(12) Rica, R.; Ziano, R.; Salerno, D.; Mantegazza, F.; van Roij, R.; Brogioli, D. Capacitive mixing for harvesting the free energy of solutions at different concentrations. *Entropy* **2013**, *15*, 1388−1407.

(13) Achilli, A.; Childress, A. E. Pressure retarded osmosis: From the vision of Sidney Loeb to the first prototype installation—Review. *Desalination* **2010**, *261*, 205−211.

(14) Lee, K.; Baker, R.; Lonsdale, H. Membranes for power generation by pressure-retarded osmosis. *J. Membr. Sci.* **1981**, *8*, 141−171.

(15) Thorsen, T.; Holt, T. The potential for power production from salinity gradients by pressure retarded osmosis. *J. Membr. Sci.* **2009**, *335*, 103−110.

(16) Yip, N. Y.; Tiraferri, A.; Phillip, W. A.; Schiffman, J. D.; Hoover, L. A.; Kim, Y. C.; Elimelech, M. Thin-film composite pressure retarded osmosis membranes for sustainable power generation from salinity gradients. *Environ. Sci. Technol.* **2011**, *45*, 4360−4369.

(17) Yip, N. Y.; Elimelech, M. Performance limiting effects in power generation from salinity gradients by pressure retarded osmosis. *Environ. Sci. Technol.* **2011**, *45*, 10273−10282.

(18) She, Q.; Jin, X.; Tang, C. Y. Osmotic Power Production from salinity gradient resource by pressure retarded osmosis: Effects of operating conditions and reverse solute diffusion. *J. Membr. Sci.* **2012**, *401*, 262−273.

(19) Kim, Y. C.; Kim, Y.; Oh, D.; Lee, K. H. Experimental investigation of a spiral-wound pressure-retarded osmosis membrane module for osmotic power generation. *Environ. Sci. Technol.* **2013**, *47*, 2966−2973.

(20) Banchik, L. D.; Sharqawy, M. H.; Lienhard, J. H. Limits of power production due to finite membrane area in pressure retarded osmosis. *J. Membr. Sci.* **2014**, *468*, 81−89.

(21) Sharqawy, M. H.; Banchik, L. D.; Lienhard V, J. H. Effectiveness-mass transfer units ($\varepsilon$-MTU) model of an ideal pressure retarded osmosis membrane mass exchanger. *J. Membr. Sci.* **2013**, *445*, 211−219.

(22) Yip, N. Y.; Elimelech, M. Thermodynamic and energy efficiency analysis of power generation from natural salinity gradients by pressure retarded osmosis. *Environ. Sci. Technol.* **2012**, *46*, 5230−5239.

(23) Post, J. W.; Hamelers, H. V. M; Buisman, C. J. N. Energy recovery from controlled mixing salt and fresh water with a reverse electrodialysis system. *Environ. Sci. Technol.* **2008**, *42*, 5785−5790.

(24) Lin, S.; Straub, A. P.; Elimelech, M. Thermodynamic limits of extractable energy by pressure retarded osmosis. *Energy Environ. Sci.* **2014**, *7*, 2706−2714.

(25) Van der Zwan, S.; Pothof, I. W. M.; Blankert, B.; Bara, J. I. Feasibility of osmotic power from a hydrodynamic analysis at module and plant scale. *J. Membr. Sci.* **2012**, *389*, 324−333.
(26) Yip, N. Y.; Elimelech, M. Comparison of energy efficiency and power density in pressure retarded osmosis and reverse electrodialysis. *Environ. Sci. Technol.* **2014**, *48*, 11002−11012.
(27) Straub, A.; Yip, N.; Elimelech, M. Raising the bar: Increased hydraulic pressure allows unprecedented high power densities in pressure-retarded osmosis. *Environ. Sci. Technol.* **2014**, *1*, 55−59.
(28) Bui, N.; McCutcheon, J. R. Hydrophilic nanofibers as new supports for thin film composite membranes for engineered osmosis. *Environ. Sci. Technol.* **2013**, *47*, 1761−1769.
(29) Song, X.; Liu, Z.; Sun, D. D. Nano gives the answer: Breaking the bottleneck of internal concentration polarization with a nanofiber composite forward osmosis membrane for a high water production rate. *Adv. Mater.* **2011**, *23*, 3256−3260.
(30) Zhang, S.; Chung, T. S. Minimizing the instant and accumulative effects of salt permeability to sustain ultrahigh osmotic power density. *Environ. Sci. Technol.* **2013**, *47*, 10085−10092.
(31) Kim, Y. C.; Elimelech, M. Adverse impact of feed channel spacers on the performance of pressure retarded osmosis. *Environ. Sci. Technol.* **2012**, *46*, 4673−4681.
(32) Skilhagen, S. E. Osmotic power—A new, renewable energy source. *Desalin. Water Treat.* **2010**, *15*, 271−278.
(33) Thelin, W. R.; Sivertsen, E.; Holt, T.; Brekke, G. Natural organic matter fouling in pressure retarded osmosis. *J. Membr. Sci.* **2013**, *438*, 46−56.
(34) She, Q.; Wong, Y. K. W.; Zhao, S.; Tang, C. Y. Organic fouling in pressure retarded osmosis: experiments, mechanisms and implications. *J. Membr. Sci.* **2013**, *428*, 181−189.
(35) Yip, N. Y.; Elimelech, M. Influence of natural organic matter fouling and osmotic backwash on pressure retarded osmosis energy production from natural salinity gradients. *Environ. Sci. Technol.* **2013**, *47*, 12607−12616.
(36) Fritzmann, C.; Löwenberg, J.; Wintgens, T.; Melin, T. State-of-the-art of reverse osmosis desalination. *Desalination* **2007**, *216*, 1−76.
(37) *Seawater Desalination Power*; White Paper; WateReuse Association: Alexandria, VA, 2011; pp 1−16.
(38) Klein, G.; Krebs, M.; Hall, V.; O'Brien, T.; Blevins, B. B. *California's Water-Energy Relationship*; Report CEC-700-2005-011-SF; California Energy Commission: Sacramento, CA, 2005
(39) Tripathi, M. *Life-Cycle Energy and Emissions for Municipal Water and Wastewater Services: Case-Studies of Treatment Plants in US*; Report CSS07-06; University of Michigan: Ann Arbor, MI, 2007.
(40) Plappally, a. K.; Lienhard V, J. H. Energy requirements for water production, treatment, end use, reclamation, and disposal. *Renewable Sustainable Energy Rev.* **2012**, *16*, 4818−4848.
(41) Song, X.; Liu, Z.; Sun, D. D. Energy recovery from concentrated seawater brine by thin-film nanofiber composite pressure retarded osmosis membranes with high power density. *Energy Environ. Sci.* **2013**, *6*, 1199−1210.
(42) Loeb, S. Production of energy from concentrated brines by pressure-retarded osmosis I. Preliminary technical and economic correlations. *J. Membr. Sci.* **1976**, *1*, 49−63.